Published in final edited form as:
Biochemistry. 2007 September 4; 46(35): 10122–10129. doi:10.1021/bi7009635.

Characterization of dihydro-A2PE: an Intermediate in the A2E Biosynthetic Pathway†

So R. Kim‡, **Jiangtao He**§, **Emiko Yanase**‡,§, **Young P. Jang**‡, **Nina Berova**§, **Koji Nakanishi**§, and **Janet R. Sparrow***,‡,¶

‡*Department of Ophthalmology, Columbia University, New York, New York 10032*

¶*Department of Pathology and Cell Biology , Columbia University, New York, New York 10032*

§*Department of Chemistry, Columbia University, New York, New York 10032*

Abstract

Bisretinoid lipofuscin pigments that accumulate in retinal pigment epithelial cells are implicated in the etiology of several forms of macular degeneration including juvenile onset Stargardt disease, Best vitelliform macular degeneration and age-related macular degeneration. One of these compounds, A2E, is generated by phosphate hydrolysis of a phosphatidylpyridinium bisretinoid (A2PE) that forms within photoreceptor outer segments. Here we demonstrate that the formation of the aromatic pyridinium ring of A2PE follows from the oxidation of a dihydropyridinium intermediate. Time-dependent density functional theory calculation, based on the structure of dihydro-A2E, produced a simulated UV-visible absorbance spectrum characterized by maxima of 494 and 344 nm. Subsequently, a compound exhibiting similar UV-visible absorbance maxima (λ_{max} 490 and 330 nm) was identified in the A2E biomimetic reaction mixture. By liquid chromatography-mass spectrometry (LC-MS) this bischromophore had the expected mass of the dihydro-pyridinium bisretinoid. The compound also exhibited the behavior of a biosynthetic intermediate, since it formed in advance of the final product A2E and was consumed as A2E accumulated. Moreover, under deoxygenated conditions, conversion to the aromatic pyridinium bisretinoid was inhibited. Taken together, these findings indicate that A2E biosynthesis involves the oxidation of a dihydropyridinium intermediate dihydro-A2PE. An understanding of the biosynthetic pathways of retinal pigment epithelial lipofuscin pigments is critical to the development of therapies for macular degeneration that are based on limiting the formation of these damaging compounds.

A number of observations over the years have shown that the deposition of lipofuscin fluorophores in RPE is dependent on the availability of vitamin A and/or vitamin A derivatives. For instance, *Rpe65* null mutation (1), amino acid variants in *Rpe65* (2), antagonists of RPE65 (3) and retinoids (13-cis retinoic acid) that inhibit 11-cis retinol dehydrogenase (4,5), all of which slow the visual cycle and reduce the flux of all-*trans*-retinal, also limit the formation of RPE lipofuscin. In addition, RPE lipofuscin accumulation in normal rat retina can be reduced by dietary vitamin A deficiency (6,7), while pharmacological agents that reduce serum vitamin A also decrease RPE lipofuscin in mice (8).

†The studies were funded by National Institutes of Health Grant EY 12951, the Steinbach Fund, Research to Prevent Blindness and the Kaplen Fund. JRS is a recipient of an Alcon Research Institute Award.

*To whom correspondence should be addressed. 630 W. 168th Street, New York NY 10021; Phone: (212) 305−9944. Fax: (212) 305 −9638. E-mail: jrs88@columbia.edu.

SUPPORTING INFORMATION AVAILABLE Cartesian coordinates and stick models of conformers used in the calculation of UV-visible absorbances. This material is available free of charge via the Internet at http://pubs.acs.org.

The first of the vitamin A aldehyde derivatives to be identified in RPE lipofuscin was A2E (Fig. 1), a pyridinium bisretinoid conjugate (9-12) ($C_{42}H_{58}NO$, molecular weight 592), named because it can be synthesized biomimetically from vitamin A aldehyde and ethanolamine when combined in a 2:1 ratio. Later, a C13-C14 Z-isomer of A2E (isoA2E) (Fig. 1) was identified (12), along with minor isomers having cis-double bonds at other positions (13). Confirmation of the structure of A2E was obtained by extensive nuclear magnetic resonance (NMR) studies (12) and by total synthesis (14). Other constituents of RPE lipofuscin include pigments generated via the condensation of two all-*trans*-retinal (15,16). These compounds include all-*trans*-retinal dimer (atRAL dimer) and the conjugates all-*trans*-retinal dimer-phosphatidylethanolamine (atRAL dimer-PE) and all-*trans*-retinal dimer-ethanolamine (atRAL dimer-E).

We previously proposed an A2E biosynthetic cascade (12,17) (Fig. 1) that is initiated with a reaction between the membrane phospholipid phosphatidylethanolamine (PE) and all-*trans*-retinal, the latter being generated upon photoisomerization of 11-*cis*-retinal (Fig. 1). We demonstrated by mass spectrometry analysis (17) that the compound formed by this reaction is the Schiff base conjugate, N-retinylidene-phosphatidyl-ethanolamine (NRPE) while others showed that NRPE is probably the ligand for ABCA4 (ABCR) (18-20), the photoreceptor-specific ATP-binding cassette transporter that is mutated in recessive Stargardt disease (21). We suggested that reaction with a second molecule of all-*trans*-retinal, would lead to the formation of a phosphatidyl dihydropyridinium molecule (dihydro-A2PE) that we envisioned would undergo automatic oxidative aromatization to yield A2PE, a phosphatidyl pyridinium bisretinoid. Although the formation of dihydro-A2PE was not, at that time, corroborated, mass spectrometry was utilized to confirm the structure of A2PE (17) and experiments demonstrating the release of A2E upon phospholipase D-mediated cleavage of A2PE established A2PE as the immediate precursor of A2E (13,17).

Since an understanding of A2E biosynthesis is essential to efforts aimed at limiting the formation of this lipofuscin pigment, we have revisited our A2E biogenesis scheme, with the aim of providing evidence for the formation of the dihydropyridinium intermediate, dihydro-A2PE. This transitional compound is of interest to us because it is likely the last intermediate before stable compound is generated. Dihydropyridinium compounds, such as dihydro-A2PE, are notoriously unstable and undergo automatic oxidative aromatization (22); thus to aid in the identification of dihydro-A2PE in our reaction mixture, we first obtained computer simulations of the UV-visible absorbance spectrum of the compound using TDDFT (23,24). In subsequent experiments we sought for evidence of a compound with similar UV-visible spectra and identical mass.

EXPERIMENTAL PROCEDURES

Time-dependent density functional theory (TDDFT): geometrical optimization of model compounds

The initial conformers of dihydro-A2E and all-*trans*-retinal ethanolamine (atRAL dimer-E) were generated by Spartan 02 software (Wavefunction Inc., Irvine CA) using the Monte Carlo method and their geometries were optimized with Merck Molecular Force Field (MMFF). Further optimization was achieved using density functional theory at the B3LYP/6−31G* level implemented using a Gaussian 03 software package (25). Two stable conformers were found for each of the structures; Cartesian coordinates (Table S1) and stick models (Figures S1, S2) are presented in Supporting Information. The Gibbs energy differences between the two conformers were 8.50 kJ/mol for dihydro-A2E and 7.54 kJ/mol for atRAL dimer-E *in vacuo*. The conformer populations were calculated by Boltzmann distribution. Since for both dihydro-A2E and atRAL dimer-E, the high-energy conformers constituted less than 5% of the total population of conformers, the contribution of the high energy conformers to the overall spectra

could be neglected. Accordingly, for the calculations of UV-visible spectra, only the lowest energy conformers were used. The experimental UV-visible absorbance spectra utilized for atRAL dimer-E was that obtained using a Jasco V530 UV-visible spectrometer with synthesized authentic standard in acetonitrile.

A2E synthetic reaction

A mixture of all-*trans*-retinal (300 μg, 2 equivalents) and ethanolamine (32 μg, 1 equivalent) in ethanol (3 ml) was stirred in the presence of acetic acid (0.3 μl) at room temperature in a capped vial in the dark for the indicated periods of time. For experiments involving synthesis under normal air and deoxygenated conditions, reaction mixtures consisting of all-*trans*-retinal (3 mg), ethanolamine (320 μg), ethanol (6 ml) and acetic acid (3 μl) were either purged or were not purged with argon, before the vessel was closed.

HPLC

An Alliance system (Waters, Corp, Milford, MA) equipped with 2695 Separation Module, 2996 Photodiode Array Detector, a 2475 Multi Fluorescence Detector and operating with Empower® software was used for HPLC analysis. An Atlantis® dC18 column (3 μm, 4.6 × 150 mm, Waters, USA) was employed. A gradient of acetonitrile and water (85% acetonitrile/15% water → 100 % acetonitrile for 15 min; 0.8 ml/min) with 0.1 % of TFA was used for mobile phase. Integrated peak areas were determined using Empower® software.

Liquid-chromatography-mass spectrometry (LC-MS)

LC-MS analysis of the reaction mixture was performed on a Quantum TSQ Discovery mass spectrometer (Thermo Electron, San Jose CA) equipped with Surveyor autosampler, Surveyor mass spectrometry pump and Surveyor PDA detector. Ten microliters of sample solution was loaded onto the column and eluted isocratically (mobile phase containing 95% acetonitrile, 5% water, and 0.1% formic acid). The column (Atlantis® dC18) was heated at 30°C and the flow rate was 0.3mL/min. The mass spectrometer was operated in positive ion mode with spray voltage at 4.0 kV and ion transfer tube temperature at 300°C. The Q1 quadrupole scans from m/z 100 to 1000 with unit resolution.

RESULTS

Calculation of UV-visible absorbance spectra of dihydro-A2PE/dihydro-A2E by time-dependent density functional theory (TDDFT). To aid in the identification of dihydro-A2E in the A2E biomimetic reaction mixture (12), we first obtained computer simulations of the UV-visible absorbance spectrum of dihydro-A2E using TDDFT (23,24). Calculations were based on dihydro-A2E rather than dihydro-A2PE, since the phospholipid moiety does not make a contribution to the UV-visible absorbance greater than ~250 nm.

Since the selection of both the functional and basis set is critical to the UV prediction, we employed two different functionals, namely B3LYP and BHandHLYP, and two different basis sets, 6−31G* and 6−31+G*, to calculate the UV-visible spectra. The BHandHLYP is a hybrid functional which combines Beck's half and half (BHandh) exchange functional (26) with Lee-Yang-parr (LYP) correlation functional (27). As compared to the B3LYP functional, the BHandHLYP functional increases the Hatree-Fock energy exchange contribution. This increase can better handle a situation which involves electron dissociation (28) or excited electronic states of delocalized pi-systems (29). The 6−31G* basis set is a polarized split-valence basis set that accommodates changes in orbital size and shape in response to a variation in the electron environment. In the 6−31+G* basis set, the diffuse function (+ sign) is added to the heavy atoms in the system. Basis sets with diffuse functions are of value for systems in

which electrons may be far from the nucleus. As such, diffuse functions more accurately reflect electron excited states such as occurs with the absorbance of UV and visible light (30).

We employed the B3LYP functional across the 6−31G* and 6−31+G* basis sets. However, the addition of the diffuse function did not significantly change the calculated UV-visible absorbance (31,32). This finding probably reflects the fact that the electron configuration in cations (such as A2E, dihydro-A2PE, dihydro-A2E; Fig. 1) is more compact and as a result can be described by smaller basis sets than are required to describe neutral molecules and anion. Thus to reduce the calculation time, only the 6−31G* basis set was used with the BHandHLYP functional to predict the UV-visible spectra. Accordingly, using the B3LYP functional across 6−31G* and 6−31+G* basis sets and the BHandHLYP functional across the 6−31G* basis set, spectra were calculated for dihydro-A2E (Fig. 2). All of the theoretically obtained spectra for dihydro-A2E had similar shapes and the differences between the two maxima (Δλ) were similar for all the calculations. Calculation at the BHandHLYP/6−31G* level, gave a simulated dihydro-A2E spectrum characterized by absorbance maxima at 494 and 344 nm (Δλ, 150 nm) (Table 1).

As a test of the validity of the functional and basis sets utilized, we also applied these geometrical optimizations to estimate the absorbance spectrum of a compound for which an experimentally derived spectrum was available. For this purpose we chose atRAL dimer-E, a bis-retinoid RPE lipofuscin pigment, the structure of which has been corroborated by ^{1}H NMR spectroscopy (16). Dihydro-A2E (molecular mass, 594) and atRAL dimer-E (Fig. 2) have the same molecular mass of 594 but differing numbers of double-bond conjugations (dihydro-A2E: 6 on the long arm, 5 on the short arm; atRAL dimer-E: 7 on the long arm, 4 on short arm); therefore, it was expected that the UV-visible spectra of these compounds would be different. On the other hand, given that they have similar polyene structures terminating in β-ionone rings, we reasoned that the geometrical optimizations (functionals and basis sets) providing calculated spectral positions closest to the values observed experimentally for atRAL dimer-E, would best estimate the absorbance spectrum of dihydro-A2E. Thus quantum chemical simulations of UV-visible absorbance spectra of atRAL dimer-E were also performed using TDDFT. The theoretically calculated UV-absorbance spectrum of atRAL dimer-E was compared to the experimentally derived spectrum determined using synthesized atRAL dimer-E.

The comparison between the experimentally-derived UV-visible spectrum and TDDFT predicted spectra for atRAL dimer-E is shown in Figure 2. All of the theoretically obtained UV-absorbance spectra for atRAL dimer-E had similar shapes. The peak positions in the B3LYP/6−31G* predicted spectrum were red-shifted relative to the peak positions measured experimentally, a difference which is typical of this theoretical approach (33). The B3LYP/6−31+G* predicted spectrum was very similar to the B3LYP/6−31G* predicted spectra, indicating, as discussed above, that the diffuse-function-containing basis set did not have a significant impact on the predicted UV-visible spectra of this structure. The BHandHLYP/6−31G* predicted spectrum was different from the other two predicted spectra and the peak positions in the BHandHLYP/6−31G* predicted spectrum were closer to the peak positions determined experimentally. A quantitative comparison between the predicted peak position for atRAL dimer-E and the experimental peak position is presented in Table 1. For atRAL dimer-E, the wavelength differences between the two peak positions (Δλ) were very similar for the three predicted spectra (Δλ, 225−227 nm) and in good agreement with the experimental data (Δλ 221 nm).

HPLC analysis of A2E biosynthetic reaction mixture

Guided by the UV-visible absorbance maxima calculated for dihydro-A2E, we next undertook to detect a compound with similar absorbance in the A2E synthetic reaction mixture of all-

trans-retinal and ethanolamine. While PE and all-*trans*-retinal are the precursors of A2E *in vivo*, in these experiments ethanolamine, instead of PE, was used as starting material because condensation of ethanolamine with all-*trans*-retinal is more facile and thus affords more reaction product; moreover, as discussed above, the phospholipid moiety does not contribute to absorbances above ~250 nm. Thus, the findings are applicable to dihydro-A2PE (molecular mass of dihydro-dipalmitoyl-A2PE, 1225). To slow the rate of A2E synthesis, the concentration of starting materials was reduced (1:10) from that typically used for A2E biomimetic synthesis. Monitoring the reaction mixture by reverse phase HPLC using a gradient of acetonitrile and water (with 0.1% TFA) revealed a peak that had a retention time of ~10.9 minutes, eluted after A2E and exhibited a UV-visible absorbance spectra characterized by λ_{max} 490 and 330 nm (Fig. 3). The peak height of this fraction diminished at 3 and 7 days of incubation while the peak height of A2E (λ_{max} 440, 334) steadily increased. IsoA2E was also identified on the basis of UV-visible absorbance (λmax 428, 338) and was most prominent at 7 days of incubation.

LC-MS analysis

To obtain the mass of each eluting compound, the 1-day reaction mixture was analyzed by LC-MS using an isocratic gradient of acetonitrile and water with 0.1% formic acid. As shown in Figure 4, the total ion chromatogram revealed signals from three eluting compounds with retention times 6.49−7.22. Operating in selected ion monitoring mode at m/z 592, 2 prominent peaks were visible that on the basis of expected mass, could be identified as A2E (all-*trans*-A2E, 6.49 min) and isoA2E (C13-C14 *Z*-isomer , 7.22 mins). Other minor peaks indicated the presence of additional A2E *cis*-isomers (6.46 and 7.82 mins) (13). Note that all of these A2E isomers have a mass of 592. With detection at m/z 594, the expected mass of dihydro-A2E, a major peak eluting between A2E and isoA2E (retention time 6.81 mins), was also detectable.

Oxidation of the dihydro-pyridinium intermediate

To test for an oxidation step in the conversion of dihydro-A2PE to A2PE, we next carried out the biomimetic synthesis of A2E under both normal air and deoxygenated (argon) conditions. Again the starting compounds were all-*trans*-retinal and ethanolamine and separate reaction mixtures were incubated in parallel to permit independent analysis at 1, 4 and 8 hours and 1, 3 and 7 days. After 1-hour incubation under normal conditions, a peak attributable to dihydro-A2E (λ_{max} 490 and 330 nm) was visible without evidence of peaks representing A2E and isoA2E; the dihydro-A2E peak continued to increase in height at 1 and 2 days of incubation but decreased by 3 days (Fig. 5). Moreover, under conditions of normal air, peaks attributable to A2E and isoA2E were not apparent until 4 hours of incubation but A2E and isoA2E peak height subsequently increased at 1, 2 and 3 days of incubation. Using peak areas to estimate the relative abundance of the compounds, it was apparent that the amount of dihydro-A2E increased in advance of A2E/isoA2E and up until 2 days of incubation, after which it decreased (Fig. 5). On the other hand, levels of A2E/isoA2E increased from 4 hours until 3 days.

When the synthetic reaction was performed under deoxygenated conditions (Fig. 5), the yield of the intermediate compound dihydro-A2E was augmented. Specifically, on the basis of visible peak height and computation of peak area, the intermediate dihydro-A2E increased in amount between 1 and 8 hours of reaction and continued to accumulate between 1 and 3 days. By comparison there was only little evidence of A2E formation between 1 and 8 hours of incubation; however, between 1 and 3 days of reaction, a steady increase in A2E peak area was observed (Fig. 5).

DISCUSSION

We previously proposed an A2E biosynthetic scheme whereby formation would begin with a reaction between all-*trans*-retinal and phosphatidylethanolamine (PE) leading to the Schiff base conjugate NRPE, that is reported to be the substrate recognized by ABCA4 (ABCR) (18-20), the photoreceptor-specific ATP-binding cassette transporter, mutation of which is responsible for recessive Stargardt disease (21). NRPE was postulated to undergo a [1,6]-proton tautomerization generating the phosphatidyl analogue of enamine. After reaction with a second molecule of all-*trans*-retinal, we suggested that an iminium salt would form and following electrocyclization, a phosphatidyl dihydropyridinium molecule (dihydro-A2PE). We envisioned that the latter molecule would undergo automatic oxidative aromatization to yield A2PE, a phosphatidyl pyridinium bisretinoid. Mass spectrometry was utilized to confirm the formation of NRPE and A2PE (17). Specifically, electrospray ionization (ESI) mass spectrometric analysis of the reaction mixture of dipalmitoyl-ʟ-□-phosphatidylethanolamine and all-*trans*-retinal, revealed prominent peaks at m/z 958.6 and 1222.9 corresponding to the protonated molecular ions of NRPE and A2PE, respectively. Moreover, fast atom bombardment tandem mass spectrometry with collision-induced dissociation mass spectrometric analysis revealed product ions *m/z* 551.4 and 408.2 for NRPE while one product ion at *m/z* 672.8 represented the phosphoryl-A2E fragment of A2PE. Additionally, the observation that incubation of A2PE with phospholipase D yields peaks in the HPLC profile that can be identified as A2E and isoA2E on the basis of UV-visible absorbance and retention time, confirmed A2PE as the immediate precursor of A2E (13,17). Several lines of investigation also demonstrated that A2PE forms within photoreceptor outer segments. For instance, the formation of [$^{14}C_2$]-A2PE has been measured in excised whole retinas following [$^{14}C_2$]-ethanolamine incorporation and irradiation to release endogenous all-*trans*-retinal. By mass spectrometric analysis it has also been shown that A2PE is the orange-colored pigment present in degenerating photoreceptor outer segment debris in Royal College of Surgeon rats (13).

The results presented here also now corroborate dihydro-A2PE as an intermediate in the biosynthetic pathway leading to A2PE and then A2E formation. This conclusion is supported by several observations. First, computer simulations of the UV-visible absorbance spectrum of dihydro-A2E using TDDFT, predicted absorbance maxima at 494 and 344 nm. Secondly, a compound exhibiting absorbance maxima (λ_{max}, 490 and 330 nm) similar to the predicted maxima was detectable within the A2E synthetic reaction mixture. This compound not only presented with the expected mass (*m/z* 594), as determined by LC-MS, it also exhibited an initial accumulation that later slowed and then decreased while A2E levels continued to rise, a pattern typical of intermediate and product, respectively, in a biosynthetic reaction.

To ascertain whether an oxidation step was involved in the conversion from dihydropyridinium to pyridinium compound, we also carried out the reaction under argon. The final product A2E formed at reduced yield under deoxygenated conditions while the dihydropyridinium intermediate steadily accumulated. This observation supports the contention that dihydro-A2PE is converted to A2PE by oxidation.

The absorbance spectrum of dihydro-A2E that was calculated by TDDFT (λ_{max} 494 and 344 nm) agrees well with the spectrum (λ_{max} 490 and 330 nm) obtained experimentally under HPLC conditions. It is worth noting that with the gradient of acetonitrile and water used for the HPLC mobile phase in these experiments, the concentration of acetonitrile at 11 minutes (approximate retention time of dihydro-A2E) would be approaching 100%. Acetonitrile is not a highly polar solvent and thus acceptable for comparing theoretical spectra calculated *in vacuo* with spectra determined experimentally. The 330 nm absorbance maxima of dihydro-A2E/dihydro-A2PE is also consistent with the peak absorbance of all-*trans*-retinol ($\Delta\lambda$325 nm). This correlation

is significant since the 330 nm absorbance is attributable to the shorter of the 2 conjugation systems in dihydro-A2E/dihydro-A2PE (Fig. 6). This conjugation system consists of 5 double bonds and terminates in a β-ionone ring; all-*trans*-retinol has the same structure and a maximum absorbance of ~325 nm. Thus the comparison between dihydro-A2E and all-*trans*-retinol lends further corroboration to the dihydro-A2E absorbance spectrum (λ_{max} 490 and 330 nm) obtained experimentally. These absorbance maxima can also be assigned to dihydro-A2PE.

In work related to RPE lipofuscin accumulation in *Abcr*$^{-/-}$ mice, a compound with absorbance maxima at 260 nm and 510 nm has been identified as dihydro-A2PE (A2PE-H_2) (5,34-37). The peak-to-peak interval between these two absorbance maxima is ~250 nm and thus substantially different than the interval (Δλ, 150 nm) we have calculated and observed experimentally for dihydro-A2E/dihydro-A2PE. In addition, we demonstrate here that the intermediate (the dihydro-pyridinium) in the A2E synthetic pathway that undergoes oxidation to yield A2PE and A2E has absorbance maxima of 330 and 490 nm. Thus our data do not support the identification of dihydro-A2PE as a 510/260 nm absorbing-species. It is also significant that in the earlier work (5,34-37), a synthesized standard of dihydro-A2PE (A2PE-H_2) was not used to corroborate the identification of the eluting compound.

In the development of novel approaches to treatment of macular degeneration, attention has been given to approaches that reduce the formation of RPE lipofuscin pigments (3-5,8). Improved understanding of the mode of genesis of A2E and other RPE lipofuscin compounds could facilitate the introduction of yet other novel approaches to therapy. In previous studies we corroborated several steps in the formation of A2E. Here, in work aimed at the further elucidation of this multi-step pathway, we demonstrate that dihydro-A2PE, a compound identifiable by absorbance peaks at 490 and 330 nm, is an intermediate in the biosynthetic pathway. An oxidation step is likely involved in the transition from dihydro-A2PE to A2PE since the dihydro-pyridinium bisretinoid intermediate accumulated in the absence of oxygen.

Supplementary Material

Refer to Web version on PubMed Central for supplementary material.

Abbreviations

AMD, age-related macular degeneration
atRAL dimer-E, all-*trans*-retinal dimerethanolamine
atRAL dimer-PE, all-*trans*-retinal dimer-phosphatidylethanolamine
DP-dihydro-A2PE, dipalmitoyl-dihydro-A2PE
DPBS, Dulbecco's phosphate buffered saline
HPLC, high performance liquid chromatography
LC-MS, liquid chromatography-mass spectrometry
NMR, nuclear magnetic resonance
NRPE, *N*-retinylidene-phosphatidyl-ethanolamine
PE, phosphatidylethanolamine
PLD, phospholipase D
RPE, retinal pigment epithelium
TDDFT, time-dependent density functional theory
TFA, trifluoroacetic acid

REFERENCES

1. Katz ML, Redmond TM. Effect of Rpe65 knockout on accumulation of lipofuscin fluorophores in the retinal pigment epithelium. Invest Ophthalmol Vis Sci 2001;42:3023–3030. [PubMed: 11687551]

2. Kim SR, Fishkin N, Kong J, Nakanishi K, Allikmets R, Sparrow JR. The Rpe65 Leu450Met variant is associated with reduced levels of the RPE lipofuscin fluorophores A2E and iso-A2E. Proc Natl Acad Sci U S A 2004;101:11668–11672. [PubMed: 15277666]

3. Maiti P, Kong J, Kim SR, Sparrow JR, Allikmets R, Rando RR. Small molecule RPE65 antagonists limit the visual cycle and prevent lipofuscin formation. Biochem 2006;45:852–860. [PubMed: 16411761]

4. Sieving PA, Chaudhry P, Kondo M, Provenzano M, Wu D, Carlson TJ, Bush RA, Thompson DA. Inhibition of the visual cycle in vivo by 13-cis retinoic acid protects from light damage and provides a mechanism for night blindness in isotretinoin therapy. Proc Natl Acad Sci U S A 2001;98:1835–1840. [PubMed: 11172037]

5. Radu RA, Mata NL, Nusinowitz S, Liu X, Sieving PA, Travis GH. Treatment with isotretinoin inhibits lipofuscin and A2E accumulation in a mouse model of recessive Stargardt's macular degeneration. Proc Natl Acad Sci U S A 2003;100:4742–4747. [PubMed: 12671074]

6. Katz ML, Drea CM, Robison WG Jr. Relationship between dietary retinol and lipofuscin in the retinal pigment epithelium. Mech Ageing Dev 1986;35:291–305. [PubMed: 3773574]

7. Katz ML, Eldred GE, Robison WG Jr. Lipofuscin autofluorescence: evidence for vitamin A involvement in the retina. Mech Ageing Dev 1987;39:81–90. [PubMed: 3613689]

8. Radu RA, Han Y, Bui TV, Nusinowitz S, Bok D, Lichter J, Widder K, Travis GH, Mata NL. Reductions in serum vitamin A arrest accumulation of toxic retinal fluorophores: a potential therapy for treatment of lipofuscin-based retinal diseases. Invest Ophthalmol Vis Sci 2005;46:4393–4401. [PubMed: 16303925]

9. Eldred GE, Lasky MR. Retinal age pigments generated by self-assembling lysosomotropic detergents. Nature 1993;361:724–726. [PubMed: 8441466]

10. Eldred GE, Katz ML. Fluorophores of the human retinal pigment epithelium: separation and spectral characterization. Exp Eye Res 1988;47:71–86. [PubMed: 3409988]

11. Sakai N, Decatur J, Nakanishi K, Eldred GE. Ocular age pigment “A2E”: An unprecedented pyridinium bisretinoid. J Am Chem Soc 1996;118:1559–1560.

12. Parish CA, Hashimoto M, Nakanishi K, Dillon J, Sparrow JR. Isolation and one-step preparation of A2E and iso-A2E, fluorophores from human retinal pigment epithelium. Proc Natl Acad Sci U S A 1998;95:14609–14613. [PubMed: 9843937]

13. Ben-Shabat S, Parish CA, Vollmer HR, Itagaki Y, Fishkin N, Nakanishi K, Sparrow JR. Biosynthetic studies of A2E, a major fluorophore of RPE lipofuscin. J Biol Chem 2002;277:7183–7190. [PubMed: 11756445]

14. Ren RF, Sakai N, Nakanishi K. Total synthesis of the ocular age pigment A2E: a convergent pathway. J Am Chem Soc 1997;119:3619–3620.

15. Fishkin N, Pescitelli G, Sparrow JR, Nakanishi K, Berova N. Absolute configurational determination of an all-*trans*-retinal dimer isolated from photoreceptor outer segments. Chirality 2004;16:637–641. [PubMed: 15382205]

16. Fishkin N, Sparrow JR, Allikmets R, Nakanishi K. Isolation and characterization of a retinal pigment epithelial cell fluorophore: an all-trans-retinal dimer conjugate. Proc Natl Acad Sci U S A 2005;102:7091–7096. [PubMed: 15870200]

17. Liu J, Itagaki Y, Ben-Shabat S, Nakanishi K, Sparrow JR. The biosynthesis of A2E, a fluorophore of aging retina, involves the formation of the precursor, A2-PE, in the photoreceptor outer segment membrane. J Biol Chem 2000;275:29354–29360. [PubMed: 10887199]

18. Weng J, Mata NL, Azarian SM, Tzekov RT, Birch DG, Travis GH. Insights into the function of Rim protein in photoreceptors and etiology of Stargardt's disease from the phenotype in abcr knockout mice. Cell 1999;98:13–23. [PubMed: 10412977]

19. Sun H, Molday RS, Nathans J. Retinal stimulates ATP hydrolysis by purified and reconstituted ABCR, the photoreceptor-specific ATP-binding cassette transporter responsible for Stargardt disease. J Biol Chem 1999;274:8269–8281. [PubMed: 10075733]

20. Sun H, Nathans J. Stargardt's ABCR is localized to the disc membrane of retinal rod outer segments. Nat Genet 1997;17:15–16. [PubMed: 9288089]

21. Allikmets R, Singh N, Sun H, Shroyer NF, Hutchinson A, Chidambaram A, Gerrard B, Baird L, Stauffer D, Peiffer A, Rattner A, Smallwood P, Li Y, Anderson KL, Lewis RA, Nathans J, Leppert

M, Dean M, Lupski JR. A photoreceptor cell-specific ATP-binding transporter gene (ABCR) is mutated in recessive Stargardt macular dystrophy. Nat Genet 1997;15:236–246. [PubMed: 9054934]

22. Dalvis D, Zhao Z, Castagnoli N. Characterization of an unexpected product from a monoamine oxidase B generated 2,3-dihydropyridinium species. J Org Chem 1992;57:7321–7324.
23. Preat J, Jacquemin D, Wathelet V, Andre JM, Perpete EA. TD-DFT investigation of the UV spectra of pyranone derivatives. J. Phys. Chem. A 2006;110:8144–8150. [PubMed: 16805501]
24. Casida ME, Jamorski C, Casida KC, Salahub DR. Molecular excitation energies to high-lying bound states from time-dependent density-functional response theory: Characterization and correction of the time-dependent local density approximation ionization threshold. J. Chem. Phys 1998;108:4439–4449.
25. Frisch, MJ.; Trucks, GW.; Schlegel, HB.; Scuseria, GE.; Robb, MA.; Cheeseman, JR.; Montgomery, J.; J. A.; Vreven, T.; Kudin, KN.; Burant, JC.; Millam, JM.; Iyengar, SS.; Tomasi, J.; Barone, V.; Mennucci, B.; Cossi, M.; Scalmani, G.; Rega, N.; Petersson, GA.; Nakatsuji, H.; Hada, M.; Ehara, M.; Toyota, K.; Fukuda, R.; Hasegawa, J.; Ishida, M.; Nakajima, T.; Honda, Y.; Kitao, O.; Nakai, H.; Klene, M.; Li, XY.; Knox, JE.; Hratchian, HP.; Cross, JB.; Bakken, V.; Adamo, C.; Jaramillo, J.; Gomperts, R.; Stratmann, RE.; Yazyev, O.; Austin, AJ.; Cammi, R.; Pomelli, C.; Ochterski, JW.; Ayala, PY.; Morokuma, K.; Voth, GA.; Salvador, P.; Dannenberg, JJ.; Zakrzewski, VG.; Dapprich, S.; Daniels, AD.; Strain, MC.; Farkas, O.; Malick, DK.; Rabuck, AD.; Raghavachari, K.; Foresman, JB.; Ortiz, JV.; Cui, Q.; Baboul, AG.; Clifford, S.; Cioslowski, J.; Stefanov, BB.; Liu, G.; Liashenko, A.; Piskorz, P.; Komaromi, I.; Martin, RL.; Fox, DJ.; Keith, T.; Al-Laham, MA.; Peng, CY.; Nanayakkara, A.; Challacombe, M.; Gill, PMW.; Johnson, B.; Chen, W.; Wong, MW.; Gonzalez, C.; Pople, JA. Gaussian, Inc.; Wallingford CT: 2004.
26. Becke AD. A new mixing of Hartree-Fock and local density-functional theories. J Chem Phys 1993;98:1372–1377.
27. Lee C, Yang W, Parr RG. Development of the Colle-Salvetti correlation-energy formula into a functional of the electron density. Phys Rev B 1988;37:785–789.
28. Zhang Y, Yang W. A challenge for density functional: self-interaction error increases for systems with a noninteger number of electrons. J Chem Phys 1998;109:2604–2608.
29. Polavarapu PL, He J, Crassous J, Ruud K. Absolute configuration of C76 from optical rotatory dispersion. Chem Phy Chem 2005;6:2535–2540.
30. Preat J, Jacquemin D, Perpete EA. Theoretical investigations of the UV spectra of coumarin derivatives. Chem Phys Lett 2005;415:20–24.
31. Hirata S, Lee TJ, Head-Gordon M. Time-dependent density functional study on the electronic excitation energies of polycyclic aromatic hydrocarbon radical cations of naphthalene, anthracene, pyrene and perylene. J Chem Phys 1999;111:8904–8912.
32. Nemykin VN, Basu P. Comparative theoretical investigation of the vertical excitation energies and the electronic structure of $[Mo^{V}0Cl_4]$-: Influence of basis set and geometry. Inorg Chem 2003;42:4046–4056. [PubMed: 12817960]
33. Cavillot V, Champagne B. Simulation of UV/visible absorption spectra of (α-diimine)nickel(II) catalysts by time-dependent density functional theory. Int J Quantum Chem 2005;101:840–848.
34. Mata NL, Tzekov RT, Liu X, Weng J, Birch DG, Travis GH. Delayed dark adaptation and lipofuscin accumulation in abcr+/− mice: implications for involvement of ***ABCR*** in age-related macular degeneration. Invest Ophthalmol Vis Sci 2001;42:1685–1690. [PubMed: 11431429]
35. Mata NL, Weng J, Travis GH. Biosynthesis of a major lipofuscin fluorophore in mice and humans with ABCR-mediated retinal and macular degeneration. Proc Natl Acad Sci U S A 2000;97:7154–7159. [PubMed: 10852960]
36. Radu RA, Mata NL, Bagla A, Travis GH. Light exposure stimulates formation of A2E oxiranes in a mouse model of Stargardt's macular degeneration. Proc Natl Acad Sci U S A 2004;101:5928–5933. [PubMed: 15067110]
37. Bui TV, Han Y, Radu RA, Travis GH, Mata NL. Characterization of native retinal fluorophores involved in biosynthesis of A2E and lipofuscin-associated retinopathies. J. Biol. Chem 2006;281:18112–18119. [PubMed: 16638746]

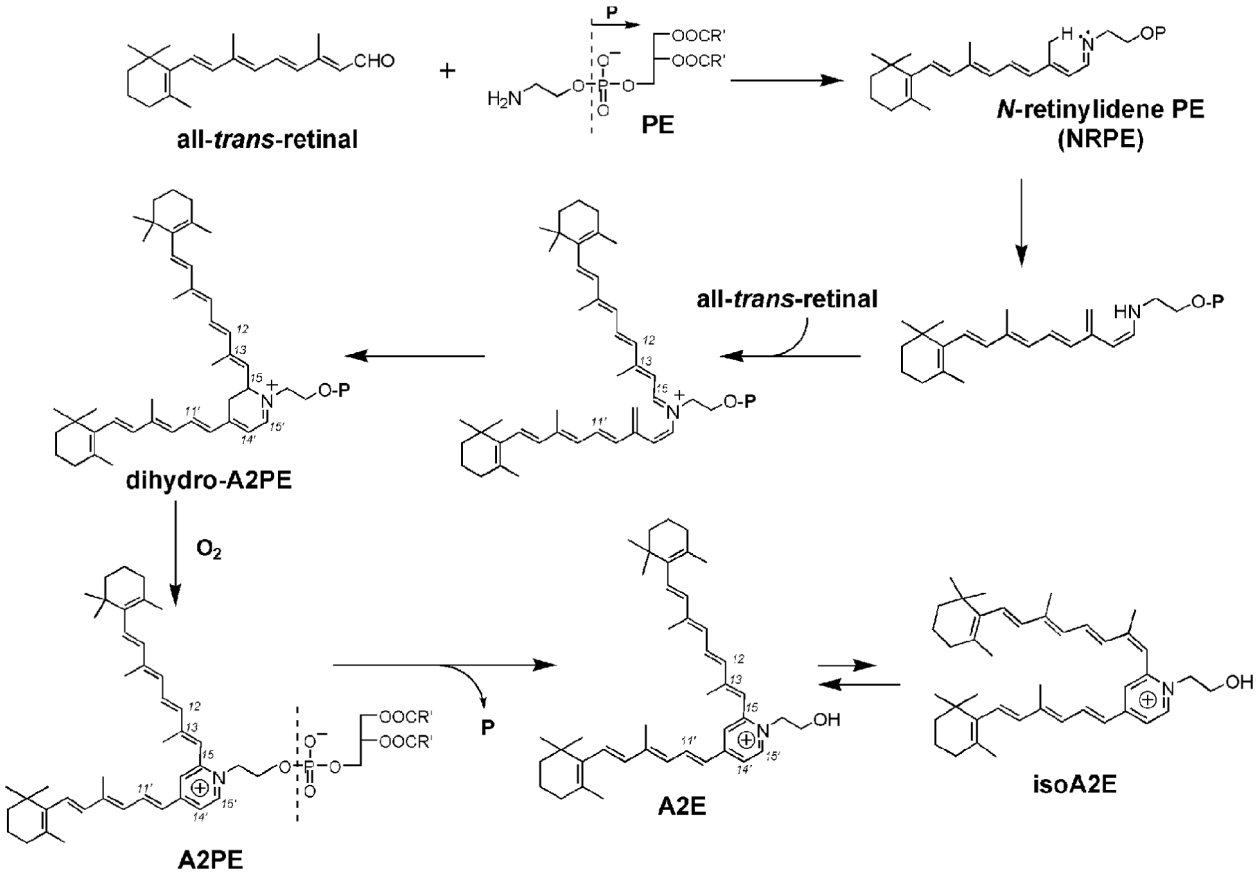

Figure 1.

Proposed biosynthetic pathway of A2E. All-*trans*-retinal that forms from photoisomerization of 11-*cis*-retinal reacts with phosphatidylethanolamine (PE) to generate the Schiff base *N*-retinylidene-phosphatidylethanolamine (NRPE). This adduct undergoes a [1,6]-proton tautomerization generating the phosphatidyl analogue of enamine which reacts with a second molecule of all-*trans*-retinal. Following 6 π-electrocyclization a dihydro-phosphatidylpyridinium bisretinoid (dihydro-A2PE) is formed and after aromatic autooxidation, A2PE is generated. Hydrolysis of the phosphate ester of A2PE yields A2E. The photoisomers A2E and isoA2E exist in photoequilibrium (4:1 ratio).

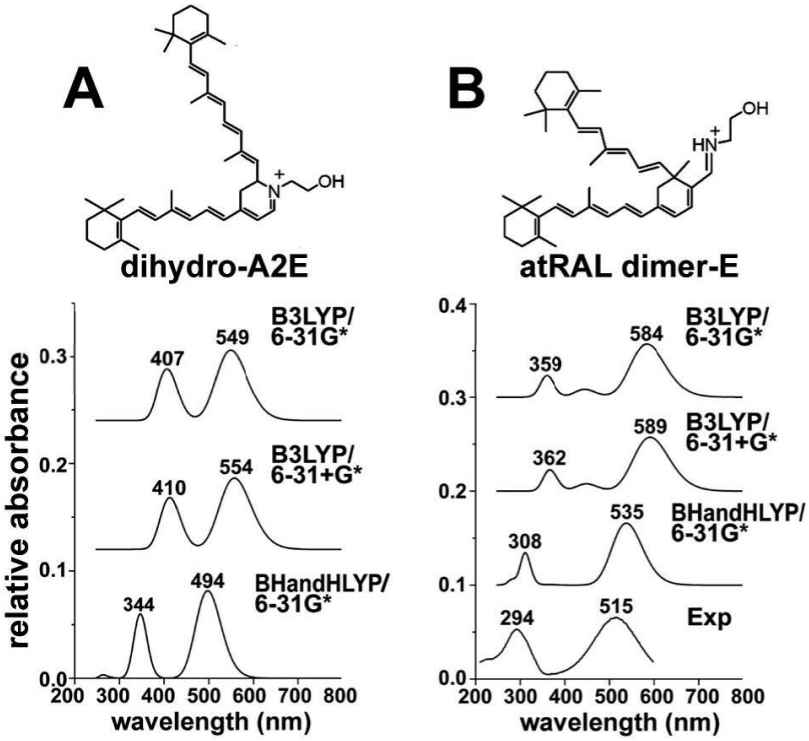

Figure 2.

Calculated UV-visible absorbance spectra of dihydro-A2E (A) and atRAL dimer-E (B) employing B3LYP and BHandHLYP functionals and 6−31G* and 6−31+G* basis sets within the TDDFT method. An experimentally-determined spectrum (Exp) for atRAL dimer-E (A) is also presented.

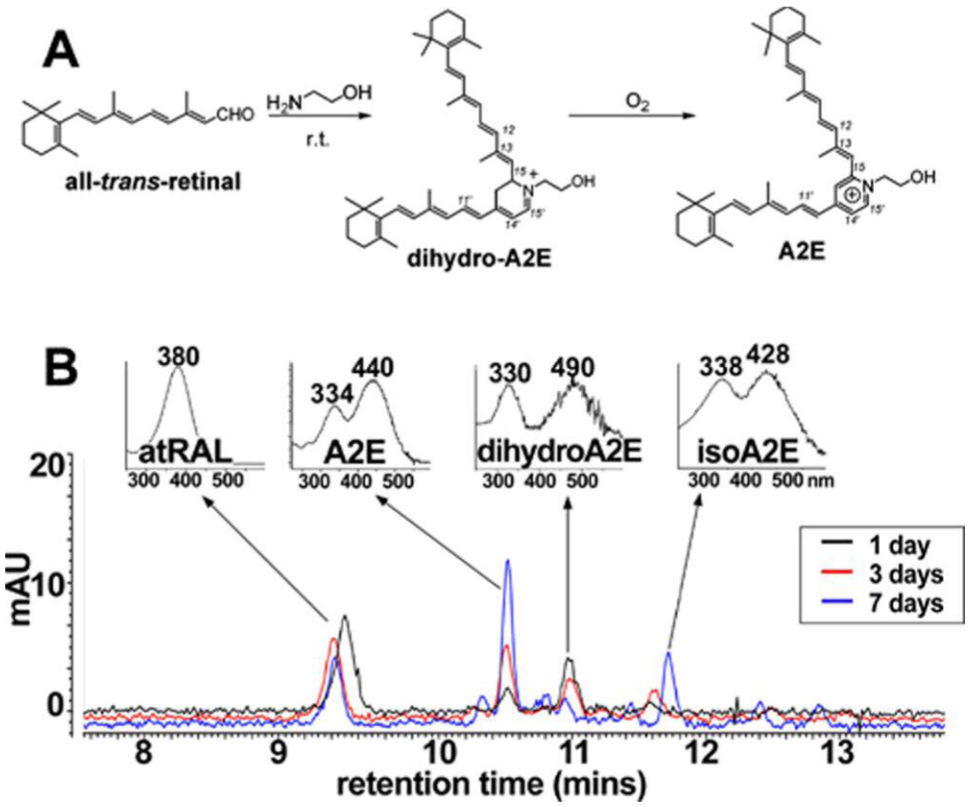

Figure 3.

Detection of a dihydropyridinium intermediate by HPLC analysis. A. Biomimetic synthesis of A2E starting from all-*trans*-retinal and ethanolamine with dihydro-A2E as intermediate. r.t., room temperature. B. HPLC monitoring of the reaction mixture of all-*trans*-retinal and ethanolamine. The reaction mixture was incubated at room temperature in the dark for 1, 3 or 7 days and the constituents of the mixture were separated by reverse phase HPLC with monitoring at 430 nm. UV-visible spectra obtained using a photodiode array detector. atRAL, all-*trans*-retinal.

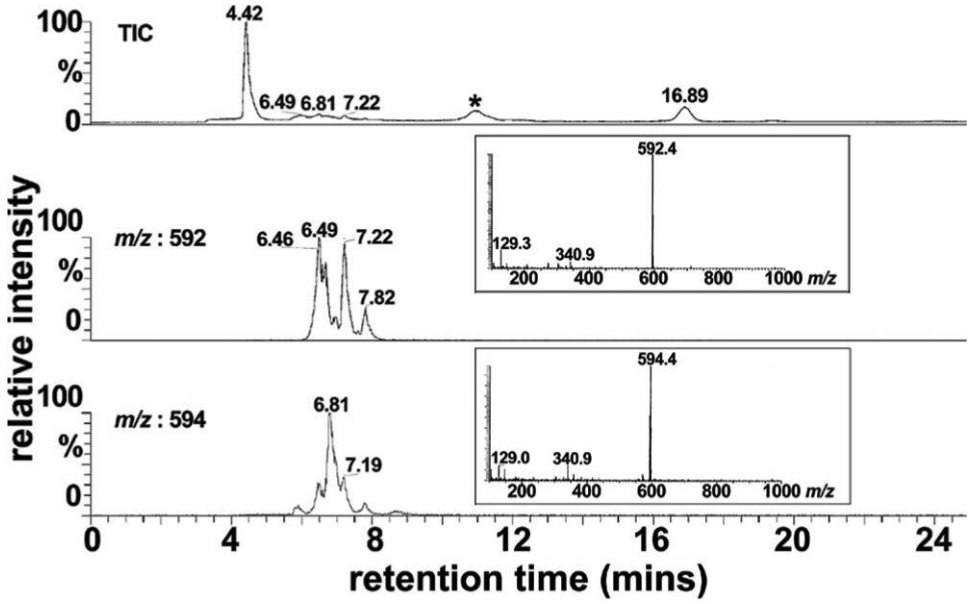

Figure 4.

LC-MS analysis of reaction mixture of all-*trans*-retinal and ethanolamine. Full scan acquisition was acquired in ESI mode, recorded as total ion current (TIC) and plotted as a function of retention time in a reversed phase HPLC column (top panel). For selected ion monitoring chromatograms, detection was set for mass to charge (*m/z*) ratios of 592 (middle panel) and 594 (bottom panel). * matrix peak. The multiple peaks in the chromatogram generated with selected ion monitoring at 592 represent A2E isomers; all of these isomers account for the single m/z peak at 592. The peak at retention time of 7.19 mins (selected ion monitoring at 594) is probably an isomer of dihydro-A2E.

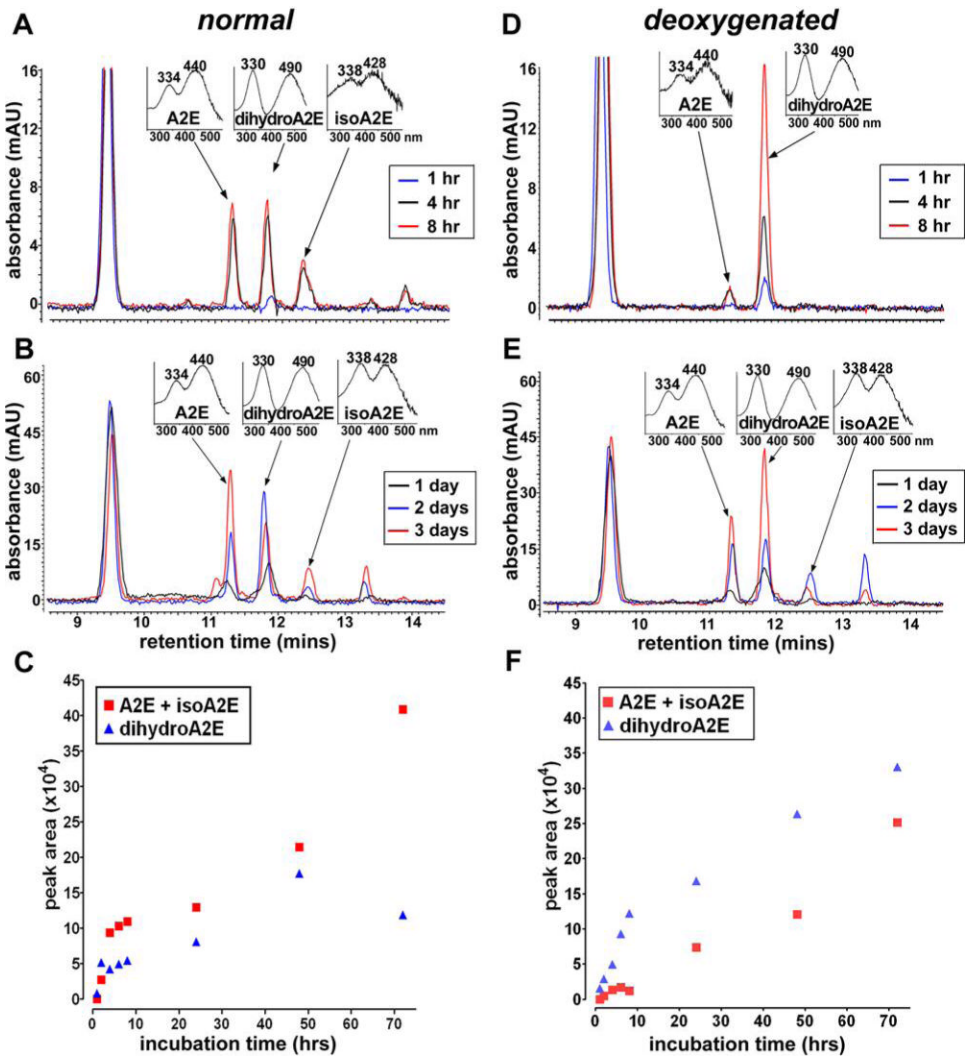

Figure 5.

An autooxidation step in the A2E synthetic cascade. A2E synthetic reaction under normal air (A-B) and deoxygenated (argon) (D-E) conditions. Starting materials were all-*trans*-retinal and ethanolamine and reaction mixtures were analyzed by reverse phase HPLC after incubation for 1, 4 and 8 hours (A and D) and 1, 2 and 3 days (B and E). Quantitation was performed by integrating chromatographic peak areas (C and F). The major peak eluting at ~9.5 minutes is all-*trans*-retinal.

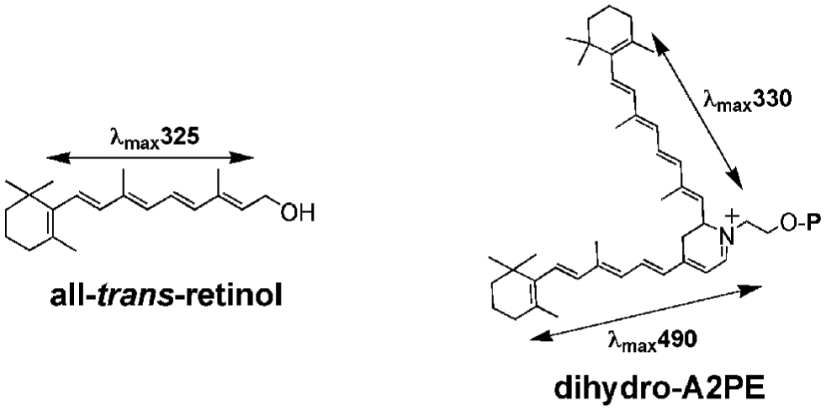

Figure 6.

Structures of all-*trans*-retinol and dihydro-A2PE. All-*trans*-retinol has an absorbance maximum at 325 nm that reflects an extended conjugation system consisting of a polyene chain of 4 double bonds with a fifth conjugated olefin in the β-ionone ring. For the bischromophore dihydro-A2PE, an absorbance maximum of 330 nm is generated by the same conjugation system.

Table 1

Absorbance maxima and the wavelength difference between absorbance peaks (Δλcalculated for dihydro-A2E[1] and atRAL dimer-E and presented in relation to functional and basis sets. For atRAL dimer-E comparison between empirically determined spectrum and predicted spectra is presented.

	dihydro-A2E			**atRALdimer-E**		
	λ_{max} **1**	λ_{max} **2**	$\Delta\lambda^2$	λ_{max} **1**	λ_{max} **2**	$\Delta\lambda^2$
Empirical[3]	—	—	—	294 nm	515 nm	221 nm
B3LYP/ 6−31G*	407 nm	549 nm	142 nm -	359 nm 22.1%	584 nm 13.4%	225 nm 1.8%
B3LYP/ 6−31+G*	410 nm	554 nm	144 nm	362 nm 23.1%	589 nm 14.4%	227 nm 2.7%
BHandHLYP/ 6−31G*	344 nm	494 nm	150 nm	308 nm 4.8%	535 nm 3.9%	227 nm 2.7%

[1] spectra calculated for dihydro-A2E are applicable to dihydro-A2PE (see text for explanation)

[2] difference between λ_{max} 1 and λ_{max} 2.

[3] determined usin nthetic samle